Composite Structures 133 (2015) 930–938

Contents lists available at ScienceDirect

Composite Structures

journal homepage: www.elsevier.com/locate/compstruct

Shape memory polymer S-shaped mandrel for composite air duct manufacturing

Haiyang Du [a,b], Liwu Liu [a], Jinsong Leng [c], Huaxin Peng [b,d], Fabrizio Scarpa [b,*], Yanju Liu [a,*]

[a] Department of Astronautical Science and Mechanics, Harbin Institute of Technology, Harbin 150001, People's Republic of China
[b] Advanced Composites Centre for Innovation and Science (ACCIS), University of Bristol, Bristol BS8 1TR, UK
[c] Centre for Composite Materials and Structures, Harbin Institute of Technology, Harbin 150080, People's Republic of China
[d] Institute for Composites Science Innovation, School of Materials Science and Engineering, Zhejiang University, Hangzhou 310027, People's Republic of China

ARTICLE INFO

Article history:
Available online 7 August 2015

Keywords:
Shape memory polymer
Composites manufacturing
Air duct
Carbon filament wound molding
Finite elements
Viscoelasticity

ABSTRACT

The work describes a concept of shape memory polymer (SMP) mandrel to manufacture a complex shaped filament wound carbon composite air duct. The mandrel is designed, fabricated and tested to verify the shape recovery and extraction characteristics for the manufacturing of the composite structure. A finite element model is developed to predict the shape recovery and overall deformation behavior due to the combination of pressure and temperature profiles used during the molding. The agreement between the deformations predicted by the finite element model and the ones measured on the SMP demonstrator are good, and show the feasibility of the smart material mandrel to be used in the production of composite structures with complex and ducted forms. A demonstrator of a PAN-carbon/epoxy filament wound composite air duct is manufactured, and the capability of the SMP mandrel verified through a hot gun extraction process.

1. Introduction

Shape memory polymers (SMPs) are a type of polymeric smart material that can maintain one temporary form and recover the original shape under external stimuli like temperature [1], light [2,3], electricity [4], magnetism [5,6] and solvents [7]. The advantages of SMPs are their ability to undergo large-deformations and their shape memory effect. However, the low mechanical properties (stiffness and strength) are in general not sufficient for structural applications, and therefore several types of reinforcements are added into the SMP matrix to produce composites with improved mechanical properties [8–10], Nowadays, SMPs and especially shape memory polymer composites (SMPCs) have been widely used in several engineering applications ranging from deployable space structures [11–13], morphing airframes [11,14] and adaptive optical [15,16], and biomedical devices [11,17]. Other applications in which SMPCs have been used include smart textiles and fabrics [11,18], smart dry adhesives [19], self-healing systems [11,20] and mandrel fabrication technologies involving recycling [21,22]. Cornerstone Research Group (CRG) have demonstrated the feasibility of using smart mandrel (bottle-shaped mandrel and air duct mandrel) based on SMP for composite manufacturing [21].

Complex 3D composite structures are often built using multi-piece mandrels. A multi-piece metal mandrel involves however a considerable amount of labour and capital time in terms of design, manufacturing and energy requirements of the manufacturing tool [21]. Moreover, some careful considerations must be given to the assembly/disassembly process to guarantee a suitable extraction of the tooling from the composite part [11,21]. Multi-piece mandrels are also quite heavy to produce large composite structures, making also difficult the transportation and relocation of the tooling if needed. Water-soluble mandrels made from a steel central support rod and sand/salt/plaster fillers are able to fabricate general composite parts with complex curvature, the fillers being used to shape the mandrel and the rob is applied to fix the mandrel for winding [23]. In general, the mandrel surfaces need to be polished and sprayed with some agent before winding. In addition, the fillers will be heavy to produce large composite structures and significant amount of water is needed to dissolve the mandrel after the fabrication of the composite structures.

The SMP deformable mandrel is a new tooling concept for mandrel-based design and production of composite structures with complex curvatures. The SMP material, which can increase its stiffness by two orders of magnitude from high temperatures (higher than the transition one) to low temperatures (lower than the transition temperature) can maintain and recover the original shape of the complex curved composite structure. Moreover, the

* Corresponding authors.
E-mail addresses: f.scarpa@bristol.ac.uk (F. Scarpa), yj_liu@hit.edu.cn (Y. Liu).

http://dx.doi.org/10.1016/j.compstruct.2015.08.005
0263-8223/

compliance of SMP under high temperatures is also an important characteristic to be used in the design of these particular mandrels. During the extraction of the composite material after curing a higher stiffness of the SMP at low temperatures can provide enough rigidity to be used as liner of the composite parts during the manufacturing process. Other advantages of the SMP-based mandrel concept is its simple fabrication and extraction process, leading to savings in both labor and production time, low weight (suitable for transport and relocation of the tooling) and recyclability of the SMP polymer, which gives some significant advantages in terms of life cycle. However, the SMP-based mandrel suffers from low values of stiffness and strength intrinsic to the SMP material properties, and does not guarantee a high surface accuracy during the filament winding process [23,24]. Moreover, the relatively low transition temperature cannot be used for curing high temperature resin-reinforced composite parts.

This work focuses on the investigation about the design, modeling and development of a S-shaped SMP air duct mandrel having a circular end cross-section and a rectangular one at the opposite end. In the paper, we focus in particular on the assessment of the deformation and recovery capability of a manufactured prototype of the SMP mandrel and the characterisation of the extraction process. Finite element simulations are also used to identify the total deformation and recover process and analyse the relationship between force and displacement. These results can provide design guidelines for the manufacturing of future designs of this innovative mandrel and moulding technique.

2. Manufacturing of the mandrel and experimental characterisation

2.1. Characterization of the SMP mechanical behaviour

A styrene-based SMP material is selected for the fabrication of the SMP mandrel due to its overall good deformation capabilities [25,26]. The SMP viscoelastic properties have been measured using a Dynamic Mechanical Analyzer (DMA) from 0.1Db-Metravib under single/dual cantilever bending mode. The temperature range used was between 20 °C and 120 °C with heating rates of 1 °C/min, 2.5 °C/min and 5 °C/min, respectively. The frequency of excitation was 1 Hz with a constant dynamic strain of 0.5%. The dimensions of the samples were 33.4 mm × 11.6 mm × 2.89 mm. The results from the experiments results are shown in Fig. 1.

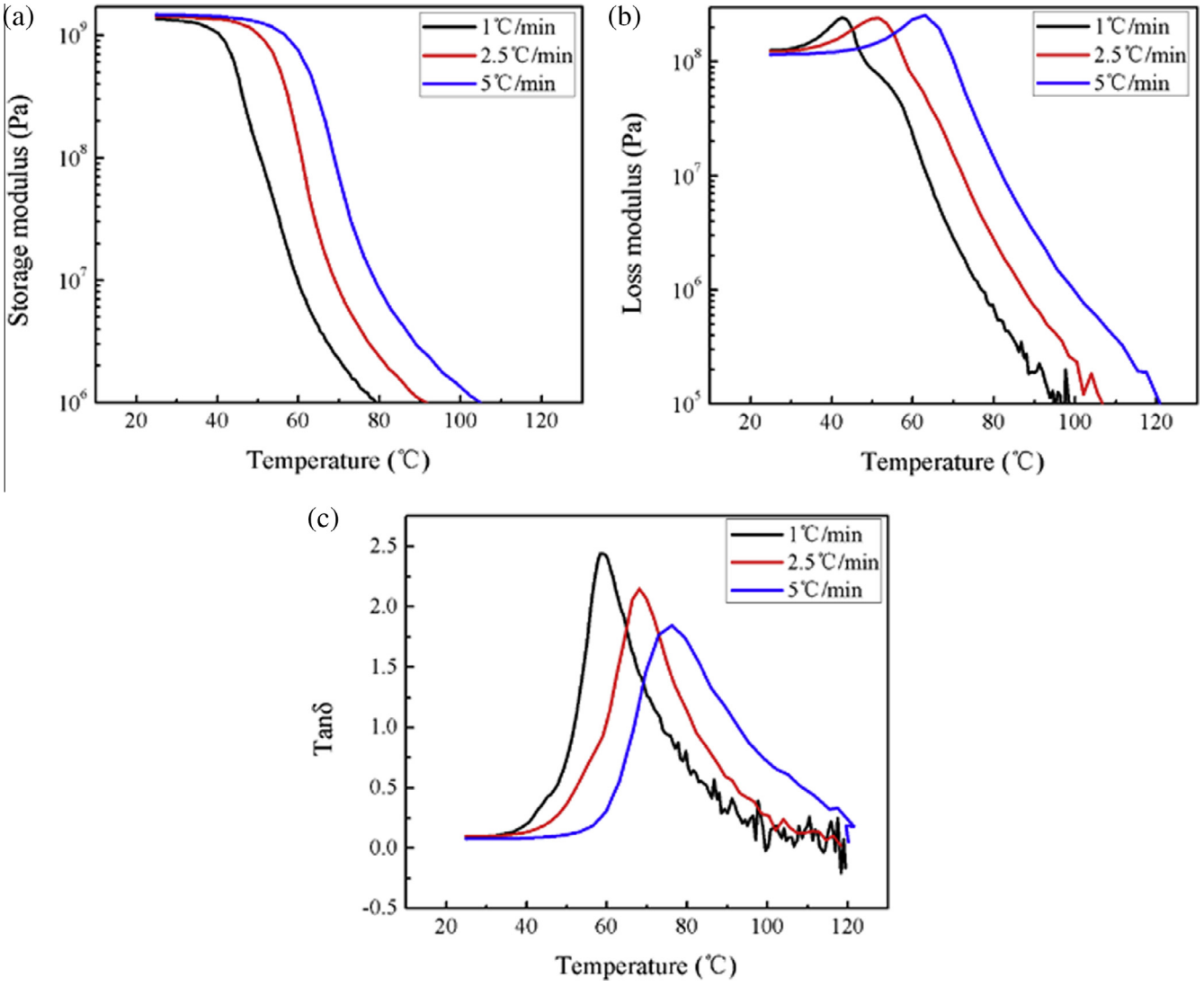

Fig. 1. Dynamic mechanical behaviour characterization of styrene-based SMP. (a) Storage modulus with different heating rate, (b) loss modulus with different heating rate, (c) Tanδ with different heating rates.

The storage modulus is shifted towards higher temperatures with the increasing of the heating rate, indicating that a rapid heating process can enhance the stiffness and the strength of the SMP materials. The peak of the loss modulus and the loss factor also moves towards higher temperatures, although the value of the peak is reduced by 28% when the heating rate is increased Similar results have been observed by Rasa et al. when investigating the effect of the heating rate on the dynamic mechanical properties of SMP estane [27]. It is apparent that the increase of the heating rate stiffens the SMP material, because the thermal conductivity of the polymer is low and allows strain recovery at larger temperature windows, similarly to what observed in epoxies and polyurethane [28,29]. In general, the peak value of the loss factor can be selected as being the transition temperature [30]. However other methods do exist to fix the transition temperature of SMP materials (peak of loss modulus [30] and peak of the deviation of the storage modulus [31]). The different transition temperatures for the styrene-based polymer used in this work are illustrated in Table 1.

2.2. Fabrication process of the SMP air duct mandrel

The fabrication process of SMP mandrel is similar to the manufacturing route used to produce inflation mandrels [32,33], the only difference being the material used in this case. The shape memory polymer replaces the traditional material (rubber and membrane-type solids) in the process of mandrel fabrication; as a consequence, the mandrel can maintain the temporary working configuration without changing the internal pressure. The fabrication of the SMP mandrel prototype is as follows. A straight tube with a length of 310 mm is considered as being the original shape of the SMP air duct mandrel (Fig. 2(a)), then the tube is placed into the outer surface of a steel mold at high temperature (Fig. 2(b)) and internal pressure is used to inflate the tube until the shape obtained is the replica of the internal surface shape. After this step the temperature is reduced to room environment and the internal pressure of the tube is removed. The final shape corresponds to the temporary working configurations (Fig. 2(c)). Finally, a filament winding process with carbon fiber and epoxy resin is carried out on the surface of the SMP air duct mandrel to produce a composite air duct.

2.3. Shape recovery process of SMP mandrel

One of the advantages of the SMP mandrel is the strong stiffness variation (higher than 100 times) between the high temperature and room temperature configurations. The mandrels possess sufficient stiffness to operate the filament winding when the temperature is lower than the glass transition one. The mandrel can recover the original tubular shape and it is easily extracted from the composite part. The shape recovery process at higher temperature (55 °C) can be observed in Fig. 3, in which the SMP mandrel cross-sections distribution is significantly modified to easy allow the extraction of the final composite part, and the shape recovery process can be finished within 150s [34].

Table 1
The transition temperature under different methods.

Heating rate °C/min	Peak of loss factor (°C)	Peak of loss modulus (°C)	Peak of the deviation of storage modulus (°C)
1.0	59.00	42.65	43.35
2.5	68.05	51.70	53.55
5.0	76.20	63.10	59.85

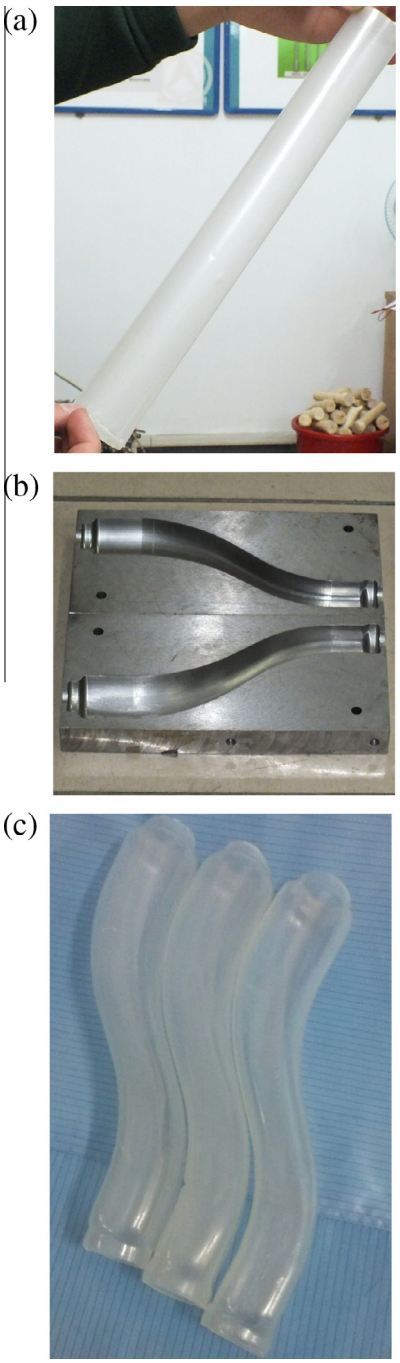

Fig. 2. Fabrication process of S-shaped SMP air duct mandrel. (a) The original configuration of the SMP air duct mandrel, (b) outer steel mold for the air duct, (c) final SMP air duct mandrels.

2.4. Verification of the extraction process

After the SMP mandrel has been fabricated using the outer steel mold, the shape recovery capability of the mandrel has been verified by the construction of a composite air duct demonstrator. A PAN-based carbon ribbon (Cangzhou Zhongli New Materials company, China) with E51 epoxy resin with curing agent phenolic amine mixed with weight ratio 4:1 (Harbin FRP Research Institute, China) has been wound on the mandrel surface following a wet winding process. The composite part has been kept under rotation and cured for 10 h at the room temper-

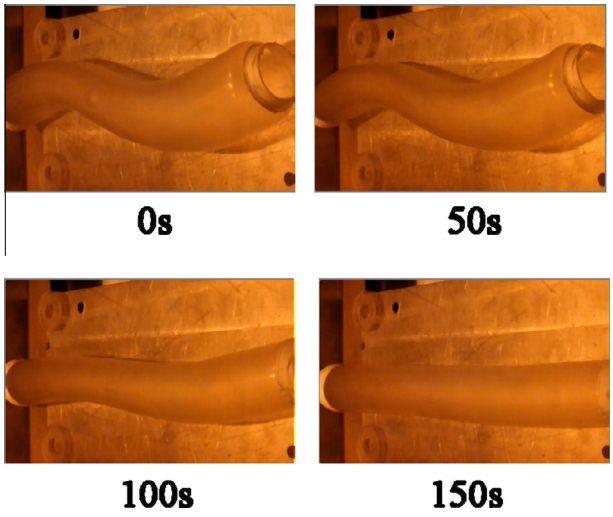

Fig. 3. Shape recovery process of S-shaped SMP air duct at 55 °C and different instants of time.

ature. The feasibility of the extraction process from the SMP mandrel has been carried out following the steps in Fig. 4. Initially the air duct-shaped composite part with internal SMP mandrel is heated above the glass transition temperature of the SMP by a heat gun set as 80 °C and maintained at the temperature for 5 min. The SMP mandrel tends to recover the original shape and debonds from the internal surface of the composite part. Finally, a small pulling force is applied one end of the SMP and the SMP mandrel is easy extracted from the composite part. The result shows that the SMP mandrel can recover the original straight tube shape and is relatively easy to extract from the composite structure. To further facilitate the extraction of the SMP mandrel from the carbon air duct after heating, a paraffin wax release agent (Hengda Material Company, China) should be painted on the surface of the mandrel.

3. Analysis of the shape memory effect in the mandrel

The analysis of the deformation in SMP materials is generally modeled using two approaches; one is based on the use of classical linear viscoelastic theory, the other adopts the phase transition theoretical model. Yu et al. predicted the free recovery behavior and multi-shape recovery behavior using a series of springs and dashpots in parallel and series, as the standard approach in linear viscoelasticity [35,36]. Diani et al. have also analyzed the free recovery behavior of SMP materials under large torsion and tensile deformation using the viscoelastic approach [37,38]. The phase transition theory states that the SMP material can be described as a combination of an active and a frozen phase. The active phase occurs when the environmental temperature is high, the material is soft, and the active phase domain represents the main part of the polymer. The frozen phase conversely describes the behavior of the polymer at low temperatures. The phase transition model was developed by Liu et al. and investigated the free and constraint recovery behavior of pure SMPs and SMP composites [39,40], Guo et al. also investigated the change of volume fraction of the frozen phase under stress for a thermally-induced SMP material [41]. Based on Diani work [38], the general Maxwell model is applied in this work to express the viscoelastic properties with time–temperature superposition properties [38,42]. The resultant relaxation modulus and time are implemented into the ABAQUS software during the shape deformation simulation. Another assumption of the modeling of the thermoforming is the presence of stresses within linear elastic regime inside the SMP mandrel shell, although the overall displacement may be nonlinear geometric. As it will be clear from the comparison between the numerical simulations and experimental results, these assumptions are sufficient to yield a good accuracy and simulation of the thermoforming process for the mandrel.

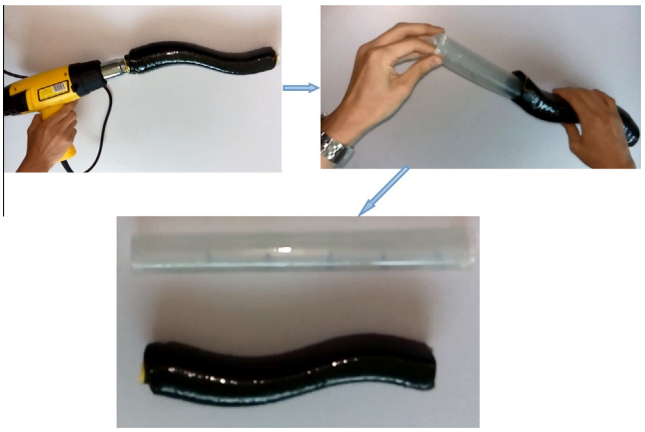

Fig. 4. Demonstration of the feasibility of extracting the SMP mandrel from the filament wound carbon air duct.

4. Simulation of the deformation and recovery of the SMP mandrel

The SMP tube is initially modeled as a curved hollow cylinder of 35 mm of diameter and 1.5 mm of thickness applied inside the mold (Fig. 5(a)). The outer steel mold is divided into two parts and assumed to be a discrete rigid wall during the simulation process. The whole assembly diagram is shown in Fig. 5(b). Due to the asymmetry existing within the two parts in the outer mold, the SMP tube will exhibit some deformation when the two sections assemble together. Also, for the purpose of this work the geometry configuration of the outer mold has been significantly simplified to reduce the CPU time required for the simulations. The outer steel mold modeled as a discrete rigid body. The inner SMP curved tube is meshed using 7938 Hexahedral elements with element type (C3D8I) after a convergence analysis. A uniform pressure (0.02 MPa) is applied on the inner surface of tube for the mandrel deformation, and at standard nonlinear Newton–Raphson solver with switch on large deformation effects has been used. The peak of the loss modulus at a heating rate of 1 °C/min has been selected as the transition temperature. Similarly to the approach shown in reference [43], the temperature corresponding to the deformation phase of the manufacturing process is set as 60 °C, while the temperature corresponding to the fixity of the temporary shape is 30 °C. Moreover, the reheating temperature to obtain the full recovery of the mandrel has been set at 75 °C. The variation of the temperature/pressure time histories during the process is shown in Fig. 6, with the total deformation and recovery process divided into five steps. Step #1 consists in the outer mold assembly process; the two separate parts combine into a closed surface within 20s from the start of the process and provide the temporary working shape of the mandrel deformation. Step #2 involves the high temperature inflation process, with the pressure increasing to 20 kPa within 10s; the cooling process is part of step #3, with the pressure kept at the maximum value and the temperature being reduced to 30 °C in 180s with a cooling rate of 10 °C/min. During the removing process (step #4) the internal pressure is quickly decreased to the initial conditions

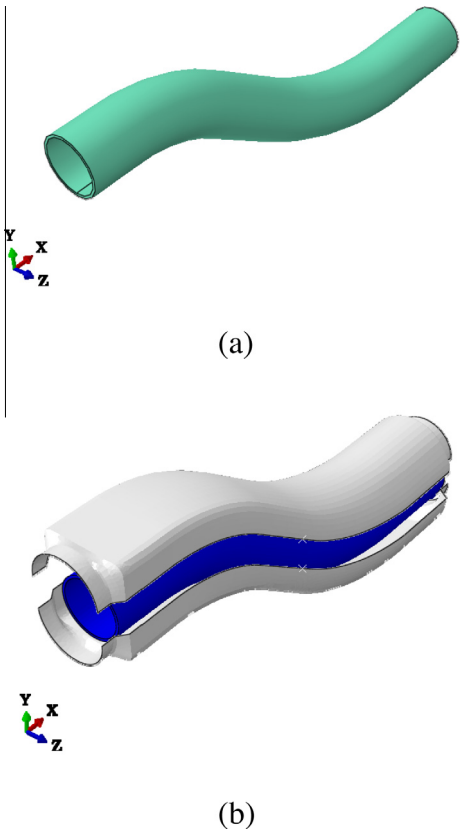

Fig. 5. Solid model of the S-shaped air duct (a). SMP curved tube. (b) Assembly between inner, outer moulds and the tube.

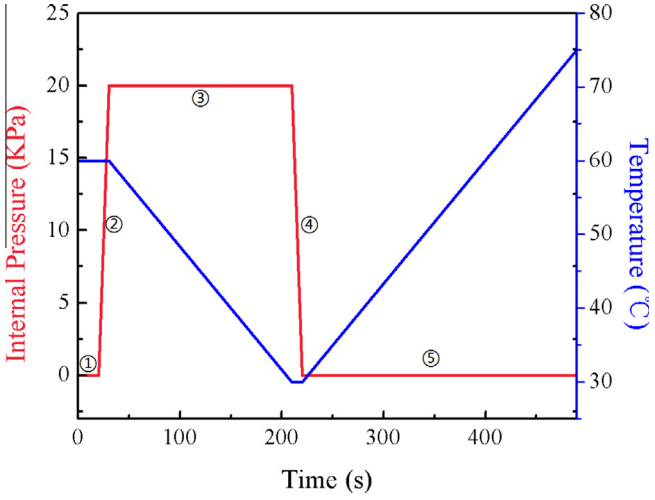

Fig. 6. Time–Temperature–Pressure diagram related to the shape programming and shape recovery processes.

in 10s. Step #5 consists in reheating the internal pressure difference kept 0 kPa and the temperature increased to 75 °C within 270s with a heating rate of 10 °C/min. Fig. 7(a) shows the distribution related to the sum of the deformations of the mandrel at beginning of the shape memory process (i.e., uniform zero displacements). When the two pieces of the outer steel are assembled together and heated after 10s the SMP tube features small displacements due to the asymmetric of the outer mold, and the shape is similar to the one present at step #1 (Fig. 7(b)). Fig. 7(c) shows the deformation of the mandrel at the end of step #3 with the outer surface of the SMP tube being a replica of internal surface of steel mold and the other end assuming a rectangular cross-section. Fig. 7(d) shows the mandrel in the cooling phase, the air duct shape structure is be kept at maximum internal pressure. After depressurization the air duct shaped mandrel assumes the fully deformed configuration (Fig. 7(e)). Fig. 7(f) shows the end of step #5 (recovery), with the air duct returning back to the original curved tube state of Fig. 7(b). It is worth of notice that there are some differences in terms of displacements distributions between the initial and final states due to the presence of residuals strains that cannot be released completely. By tracking the location of a node located on the surface of the circular section it is possible to further visualize the variation of the geometry during the shape deformation and recovery process (Fig. 8). The location of the node does not fully recover the original position when the temperature is above 60 °C, the most likely reasons are the presence of residual strains, larger automatic step sizes used by the solver for convergence and hysteresis effects given by the viscoelastic properties of the SMP material. In order to evaluate the effectiveness of the FE simulation, an air duct sample is applied on a support structure, a non-contact laser distance-measuring instrument (LK-Navigator, Kyence Company, Japan) is used to measure the recovery deformation at one point of the circular cross-section. The measurement data are stored every 20 ms. A comparison between the experimental and simulation results is shown in Fig. 8(b). The results show the good agreement between the two sets of data, and demonstrate the reliability of the FE model to predict the shape recovery effect of the SMP material.

The shape fixity and shape recovery ratio are two important factors to evaluate the shape memory effect of a SMP material [44]. A high shape fixity ratio can guarantee the surface accuracy of the mandrel, and a high shape recovery ratio can be beneficial for the extraction after curing. For a single cycle, the definition of shape fixity ratio (R_f) and shape recovery ratio (R_r) can be expressed as follows [44]:

$$R_f = \frac{L_1}{L_0} \times 100\% \tag{1}$$

where the L_0, L_1 denote the displacement of high temperature deformation and the displacement after removing force under low temperature, respectively.

$$R_r = \left(1 - \frac{L_2}{L_0}\right) \times 100\% \tag{2}$$

where L_2 denotes the residual displacement after reheating above the transition temperature. To better evaluate the deformation behavior of the SMP mandrel, the factors described in Eq. (1) and (2) have been computed by selecting the variation of the locations of specific nodes present on the two end cross-sections. The results are shown in Table 2. In addition, the mandrel thickness is also an important factor during the deformation, because an increasing thickness reduces the bending deformation with consequent higher bending stiffness. However, lower thickness values do not help to meet the maximum deformations requirements during the transformation process, and because of manufacturing imperfections the thickness is in general larger than the one prescribed at design stage [43]. The thickness change of the two end sections calculated from the FE model is presented in Table 3. It is possible to observe that the mandrel reduces its thickness by an average of 0.5 mm by measuring the node coordinate between the original state and deformed

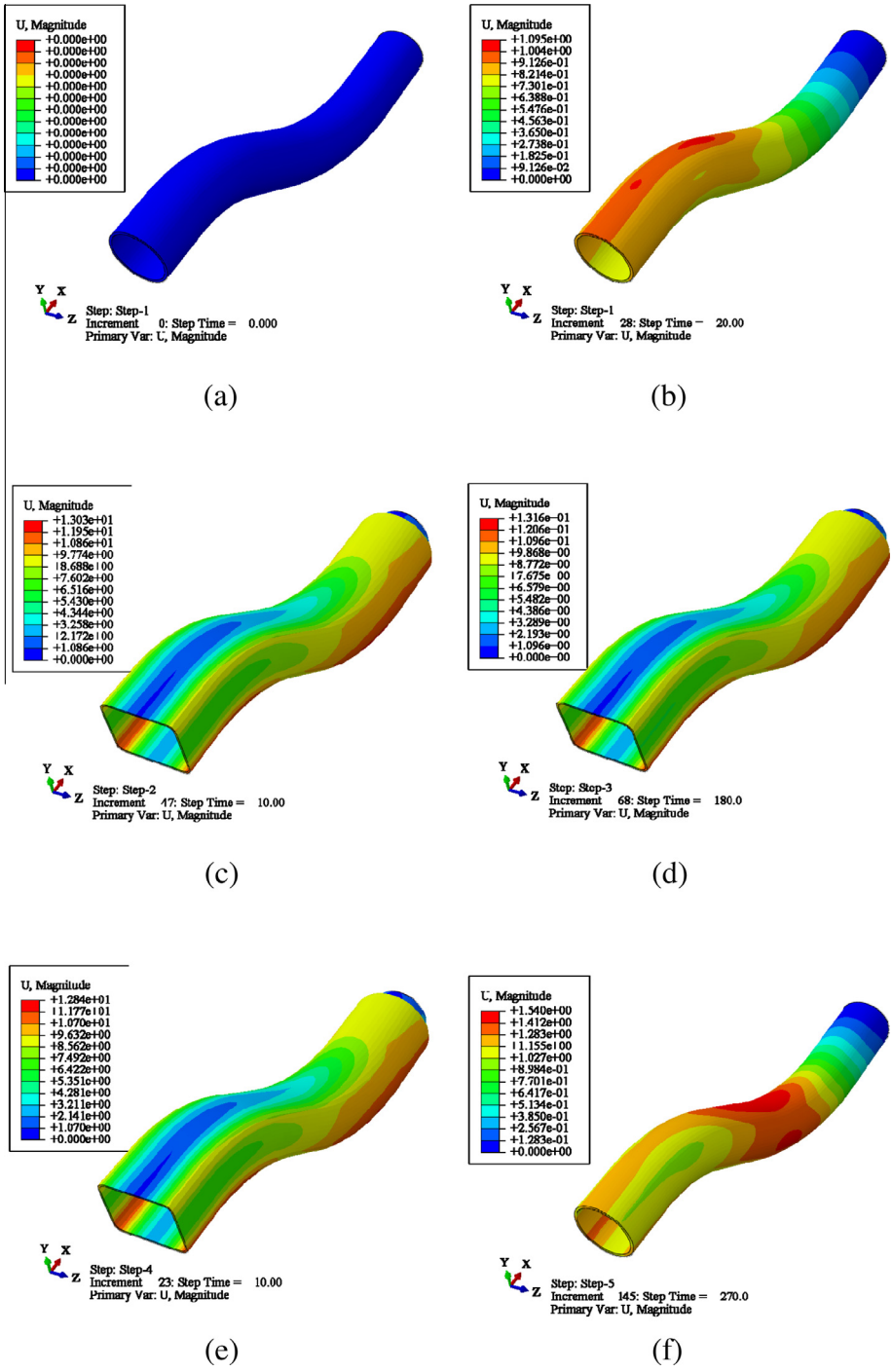

Fig. 7. Shape memory process of S-shaped air duct SMP mandrel. (a) design shape of SMP curved tube. (b) SMP tube shape after the assembly with the outer steel mold (initial shape for the simulations). (c) the shape of the tube after the high temperature deformation and (d) cooling. (e) the shape of the tube after removing the internal pressure at low temperature. (f) recovery of the tube to the initial shape using the outer mold.

state. Cooling and reheating are also two important phases of the manufacturing of the deformable mandrel, and a substantial portion of the deformations in the structure can be stored during cooling and released when reheating. The change of the configuration of the SMP tube during the reheating is shown in Fig. 9 (a) and (b) for the two end cross sections respectively. The configuration of the rectangular end cross-section does not change significantly between 30 °C and 40 °C (Fig. 9(a)). The shape of the cross section transitions to an ellipse between 40 °C and 60 °C, with the final recover assuming a circular shape from 60 °C to 70 °C. The other end of the circular cross-section also features a similar recovering process within these temperature ranges, however maintaining an overall circular shape only just reducing the diameter with the increasing temperature (Fig. 9 (b)). More details on the evolution of the SMP mandrel during the shape recovery process on specific locations of the surface can also be observed in Fig. 10. The midpoints of the two sides of the rectangular cross section (Node 6 and Node 20) and one

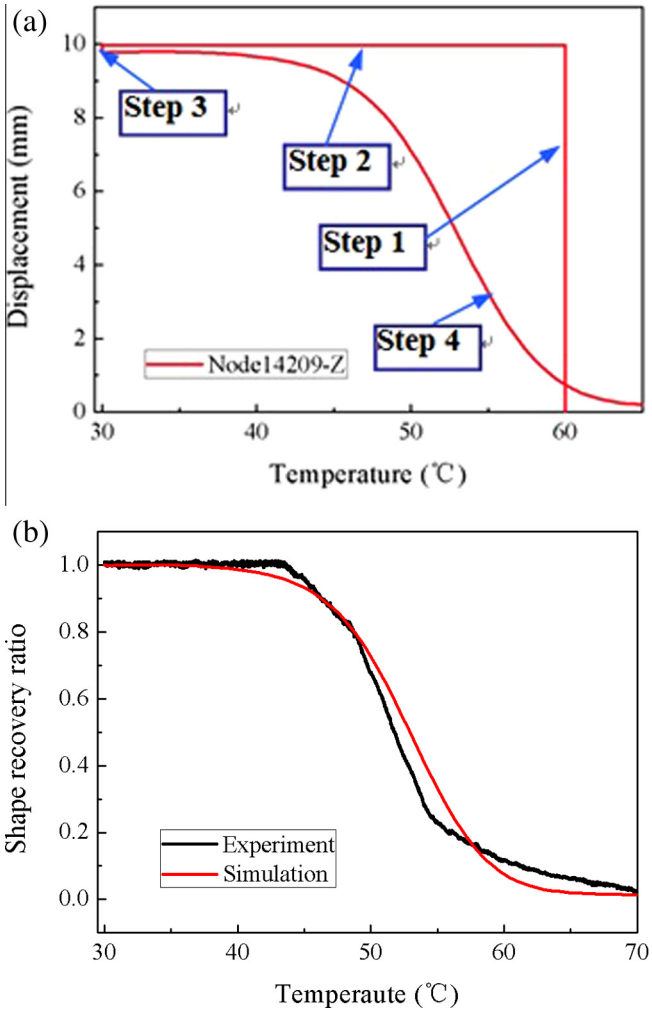

Fig. 8. Shape memory process occurring on the circular section of the tube. (a) Displacement/temperature evolution of a FE node of the section. (b) Comparison between experimental and numerical results.

Table 2
Shape fixity ratio and shape recovery ratio on two end sections.

	Y direction for rectangular section	*X* direction for rectangular section	*Y* direction for circular section
Shape fixity ratio R_f	98.2%	97.3%	98%
Shape recovery ratio R_r	97.1%	99%	97.9%

Table 3
Thickness reduction during the deformation process.

	Y direction for rectangular section	*X* direction for rectangular section	*Y* direction for circular section
Thickness change (mm)	−0.504	−0.531	−0.567

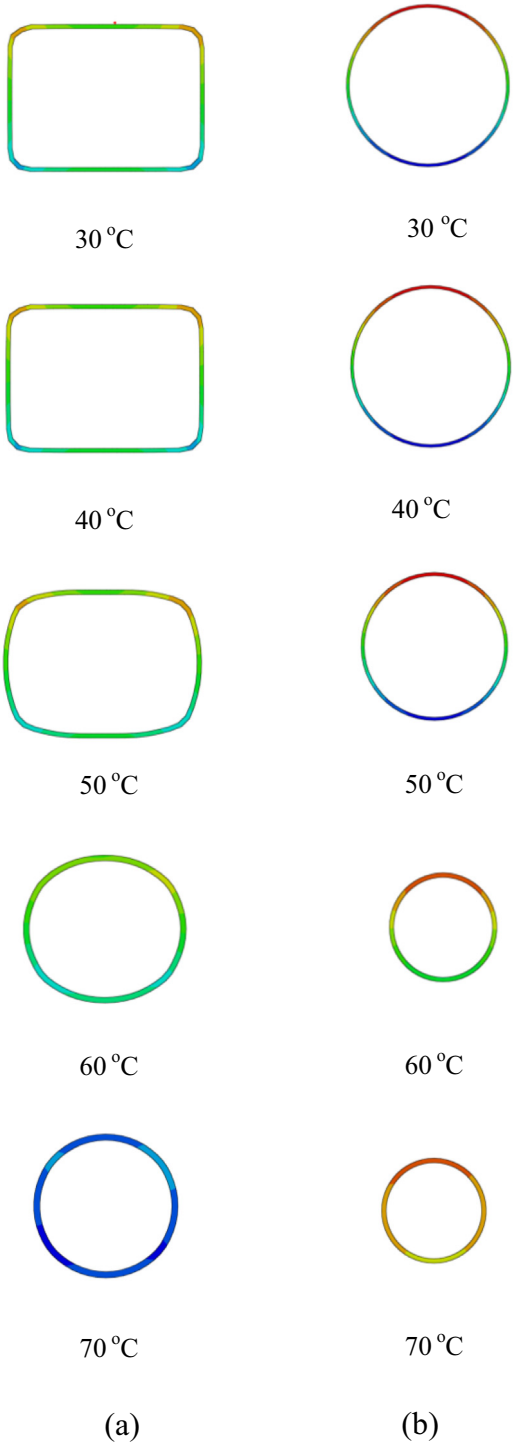

Fig. 9. Shape recovery contours of the (a) rectangular and (b) circular end cross-sections.

located to the corner (Node 15) are shown in Fig. 10(a). Similarly, three nodes are defined for the circular cross section (Fig. 10(d)). Fig. 10(b) and (e) show the displacement recovery of the mandrel during reheating. The displacement of Node 6 along the Y direction nearly remains constant, because the node is in contact with the outer stiff mold. The displacement recovery of Node 15 along the *Z*-direction tends to vary at lower temperature more than the one of the midpoint Node 20, indicating that the deformation recovery of the corner is more sensitive than the one at midpoints. The shape recovery curves are also similar during the recovery of the circular section of the SMP mandrel (Fig. 10(f)).

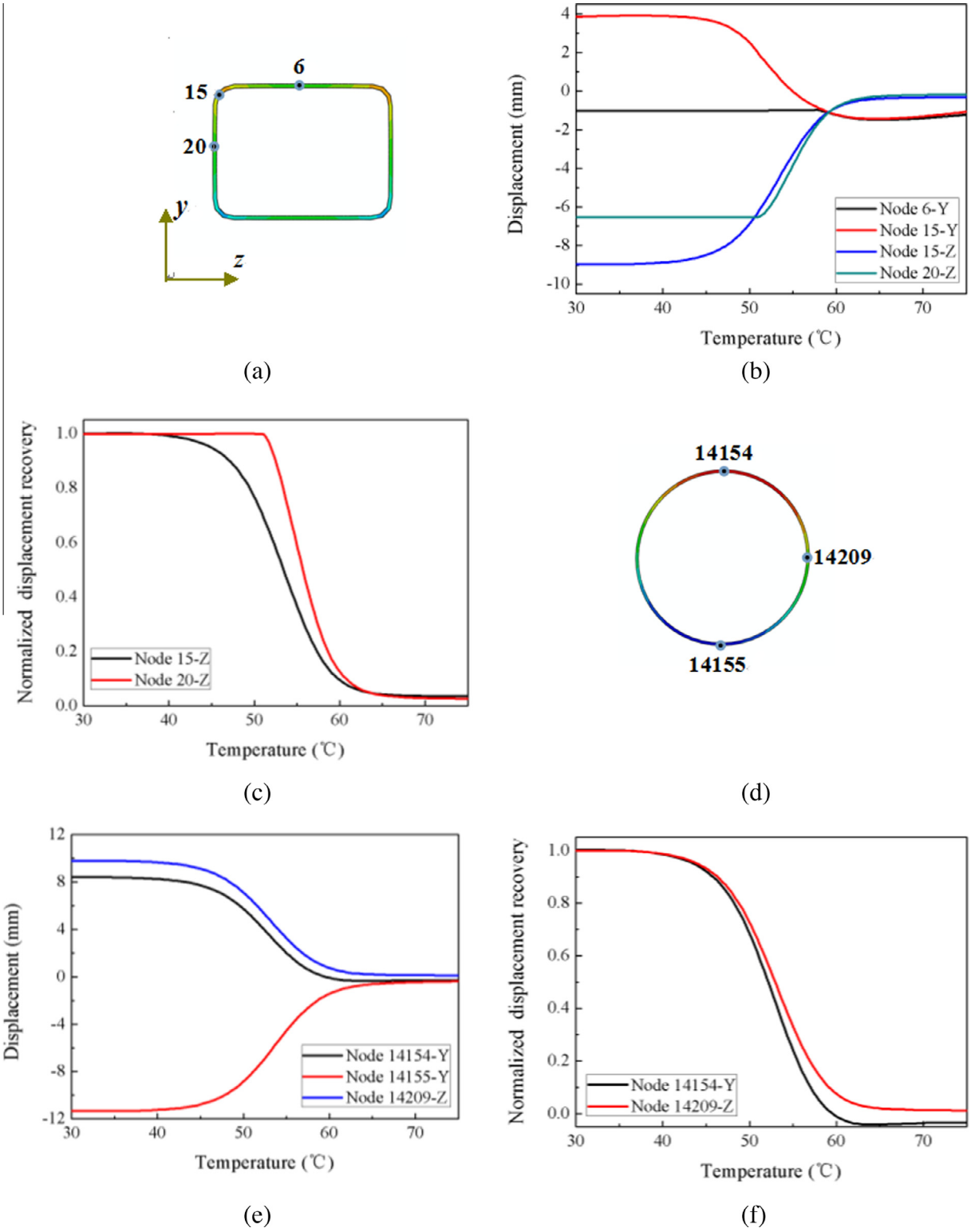

Fig. 10. Shape recovery curves of two end cross-sections. For the rectangular end: (a) location of the nodes; (b) nodes displacements along the *Y* and *Z* directions; (c) normalized displacements temperature histories. Similar graphs are for the circular cross-section (d, e, f).

5. Conclusions

This work has presented a concept of SMP air duct mandrel to replace the traditional multi-piece metal and water-soluble types currently used in the industry. The experimental and numerical results produced in the paper show that the new type of mandrel provides a high surface accuracy for the replica of the outer steel mold. Moreover, it is simple to produce, easy to extract after curing and can be more efficiently re-used compared to a traditional mandrel. An integrated constitutive model with time–temperature superposition properties has been implemented in ABAQUS to predict the shape deformation and shape recovery process of air duct

mandrel, and therefore better understand the shape memory process occurring in air duct mandrel. The results show that the constitutive model can simulate successfully the total shape memory process including the influence of the geometry, thickness changes and phase transitions. A demonstrator of an air duct carbon structure in filament winding has also been produced to show the effectiveness of the debonding from the SMP mandrel visa hot gun heating. The good agreement between the behavior predicted by the numerical model and the one measured on the demonstrator, plus the operational feasibility of extracting the SMP mandrel from the composite air duct prototype are a testimony to the reliability of the predictive tool produced and the viability of the SMP mandrel concept.

Acknowledgements

This work is supported by the National Natural Science Foundation of China (Grant Nos. 11225211, 11272106). In addition, this work is also supported by the UK-China Higher Education Research Partnership for PhD studies.

References

[1] Yu K, Ge Q, Qi HJ. Reduced time as a unified parameter determining fixity and free recovery of shape memory polymers. Nature Commun 2014;5:3066.
[2] Lendlein A, Jiang HY, Junger O, Langer R. Light-induced shape memory polymer. Nature 2005;434:879–82.
[3] Leng JS, Zhang DW, Liu YJ, Yu K, Lan X. Study on the activation of styrene-based shape memory polymer by medium-infrared laser light. Appl Phys Lett 2010;96:111905.
[4] Liu YJ, Lv HB, Lan X, Leng JS, Du SY. Review of electro-active shape memory polymer composite. Compos Sci Technol 2009;69:2064–8.
[5] Yu K, Westbrook KK, Kao PH, Leng JS, Qi HJ. Design consideration for shape memory composites with magnetic particles. J Compos Mater 2013;47:51–63.
[6] Yakacki CM, Satarkar NS, Likos R, Hilt JZ. Shape memory polymer network with Fe_3O_4 nanoparticles for remote activation. J Appl Polym Sci 2009;112:3166–76.
[7] Huang WM, Yang B, An L, Li C, Chan YS. Water-driven programmable polyurethane shape memory polymer: demonstration and mechanism. Appl Phys Lett 2005;86. 114105-1-3.
[8] Lan X, Liu YJ, Lv HB, Wang XH, Leng JS, Du SY. Fiber reinforced shape memory polymer composite and its application in a deployable hinge. Smart Mater Struct 2009;18:024002.
[9] Ni QQ, Zhang CS, Fu YQ, Dai GZ, Kimura T. Shape memory effect and mechanical properties of carbon nanotube/shape memory polymer nanocomposites. Compos Struct 2007;81:176–84.
[10] Fonseca MA, Abreu B, Goncalves FAMM, Ferrieira AGM, Moreira RAS, Oliveira MSA. Shape memory polyurethanes reinforced with carbon nanotubes. Compos Struct 2013;99:105–11.
[11] Leng JS, Lan X, Liu YJ, Du SY. Shape memory polymers and their composites: Stimulus methods and applications. Prog Mater Sci 2011;56:1077–135.
[12] Soykasap O. Deployment analysis of self-deployable composite boom. Compos Struct 2009;89:374–81.
[13] Zhang RR, Guo XG, Liu YJ, Leng JS. Theoretical analysis and experiments of a space deployable truss. Compos Struct 2014;112:226–30.
[14] Bye DR, McClure PD. Design of a morphing vehicle. In: 48th AIAA/ASME/ASCE/AHS/ASC Structures, Structural Dynamics, and Materials Conference, Honolulu, Hawaii, April, 23–26, 2007.
[15] Xie T. Tunable polymer multi-shape memory effect. Nature 2010;464:267–70.
[16] Varlese SJ, Hardaway LR. Laminated electroformed shape memory composite for deployable light weight optics. Proc SPIE: Earth Observing Syst IX 2004;5542:375–83.
[17] Wache HM, Tartakowska DJ, Hentrich A, Wagner MH. Developemnt of a polymer stent with shape memory effect as a drug delievy system. J Mater Sci Mater Med 2003;14:109–12.
[18] Hu JL, Zhu Y, Huang HH, Lu J. Recent advances in shape memory polymers: Structure, mechanism, functionality, modeling and applications. Prog Polym Sci 2012;37:1720–63.
[19] Xie T, Xiao XC. Self-peeling reversible dry adhesive system. Chem Mater 2008;20:2866–8.
[20] Meng H, Li GQ. A review of stimuli-responsive shape memory polymer composites. Polymer 2013;54:2199–221.
[21] Everhart MC, Stahl J. Reusable shape memory polymer mandrels. Proc SPIE, Smart Struct Mater: Ind Commercial Appl Smart Struct Technol 2005;5762:27–34.
[22] Zhang L, Du HY, Liu LW, Liu YJ, Leng JS. Analysis and design of smart mandrels using shape memory polymers. Compos: Part B 2014;59:230–7.
[23] Everhart MC, Nickerson DM, Hreha RD. High-temperature reusable shape memory polymer mandrels. Proc SPIE, Smart Struct Mater: Ind Commercial Appl Smart Struct Technol 2006;6171:61710K.
[24] <http://www.crgrp.com/rd-centre/smart-tooling>.
[25] Sun J, Liu YJ, Leng JS. Mechanical properties of shape memory polymer composites enhanced by elastic fibers and their application in variable stiffness morphing skins. J Intell Mater Syst Struct 2014. http://dx.doi.org/10.1177/1045389X14546658.
[26] Liu YJ, Du HY, Liu LW, Leng JS. Shape memory polymers and their composites in aerospace application: a review. Smart Mater Struct 2014;23:023001.
[27] Rasa KM, Aycan OO, Holger S. Characterization of shape memory polymer estane by means of dynamic mechanical thermal analysis technique. Smart Mater Res 2014;2014:250258.
[28] Rousseau IA, Xie T. Shape memory epoxy: composition, structure, properties and shape memory performances. J Mater Chem 2010;20:3431–41.
[29] Tobushi H, Okumura K, Hayashi S, Ito N. Thermomechanical constitutive model of shape memory polymer. Mech Mater 2001;33:545–54.
[30] Klesa IJ. Placet V, Collet M. Experimental evaluation of the rheological properties of Veriflex shape memory polymer. Master Project, Department of Applied Mechanics, Franche-Comte University, 2009.
[31] Zhou B, Liu YJ. A glass transition model for shape memory polymer and its composite. Int J Modern Phys B 2009;6–7:1248–53.
[32] Fang H, Quijano U, Bach V, Hill J, Wang KW. Experimental study of a membrane antenna surface adaptive control system. In: 52nd AIAA/ASME/ASCE/AHS/ASC Structures, Structural Dynamics and Materials Conference, Denver, CO, United States, 2011, pp. 4–7.
[33] Yang TJ, Zhang M, Zhang J. Study on mould design and process plan of the composite inlet duct. FRP/CM 2011;6:57–9.
[34] HY Du, Liu LW, Chen FL, Liu YJ, Leng JS. Design and manufacture smart mandrel using shape memory polymer. In: The 5th International Conference on Computation Methods, Cambridge, UK, 2014, pp. 28–30.
[35] Ge Q, Yu K, Ding YF, Qi HJ. Prediction of temperature-dependent free recovery behavior of amorphous shape memory polymer. Soft Matter 2012;8:11098–105.
[36] Yu K, Xie T, Leng JS, Ding YF, Qi HJ. Mechanisms of multi-shape memory effects and associated energy release in shape memory polymers. Soft Matter 2012;8:5687–95.
[37] Diani J, Gilormini P, Fredy C, Rousseau I. Predicting thermal shape memory of crosslinked polymer networks from linear viscoelasticity. Int J Solid Struct 2012;49:793–9.
[38] Arrieta S, Diani J, Gilormini P. Experimental characterization and thermoviscoelastic modeling of strain and stress recoveries of an amorphous polymer network. Mech Mater 2014;68:95–103.
[39] Liu YP, Gall K, Dunn ML, McCluskey P. Thermomechanics of shape memory polymer nanocomposites. Mech Mater 2004;36:929–40.
[40] Liu YP, Gall K, Dunn ML, Greenberg AR, Diani J. Thermomechanics of shape memory polymers: Uniaxial experiments and constitutive modeling. Int J Plast 2006;22:279–313.
[41] Guo XG, Liu LW, Liu YJ, Zhou B, Leng JS. Constitutive model for a stress- and thermal-induced phase transition in a shape memory polymer. Smart Mater Struct 2014;23:105019.
[42] Zhang YT. Theory of Thermo-viscoelastcity. Tianjin University, 2002.
[43] Zhang Lei. Design and research a smart mandrel based on shape memory polymer. Dissertation of the Master Degree in Engineering, Harbin Institute of Technology, China, 2012.
[44] Wu XL, Huang WM, Zhao Y, Ding Z, Tang C, Zhang JL. Mechanisms of the shape memory effect in polymeric materials. Polymer 2013;5:1169–202.